frontiers | Frontiers in Materials

TYPE Original Research
PUBLISHED 18 April 2024
DOI 10.3389/fmats.2024.1406045

OPEN ACCESS

EDITED BY
Xianze Cui,
China Three Gorges University, China

REVIEWED BY
Xuesen Lyu,
Hong Kong Polytechnic University, Hong Kong SAR, China
Weiwei Han,
Beijing University of Civil Engineering and Architecture, China

*CORRESPONDENCE
Zhengning Sun,
zhengning0211@163.com

RECEIVED 24 March 2024
ACCEPTED 04 April 2024
PUBLISHED 18 April 2024

CITATION
Qi G, Zhang Q and Sun Z (2024), Mechanical properties and hydration mechanism of super-sulfated cement prepared with ordinary Portland cement, carbide slag, and sodium silicate.
Front. Mater. 11:1406045.
doi: 10.3389/fmats.2024.1406045

Mechanical properties and hydration mechanism of super-sulfated cement prepared with ordinary Portland cement, carbide slag, and sodium silicate

Guangzheng Qi[1], Qiang Zhang[1] and Zhengning Sun[1,2]*

[1]National Engineering Laboratory of Port Hydraulic Construction Technology, Tianjin Research Institute for Water Transport Engineering, Tianjin, China, [2]College of Construction Engineering, Jilin University, Changchun, China

Super-sulfated cement (SSC) is known for its low-carbon footprint, energy efficiency, and eco-friendliness (mainly derived from industrial by-products) with promising applications. However, SSC's slow early strength development results in inadequate initial hardening, compromising its durability and limiting its use in practical engineering projects. This study aims to enhance SSC's early performance by incorporating ordinary Portland cement (OPC), carbide slag (CS), and sodium silicate as alkaline activators alongside anhydrite. The effects of varying proportions of OPC, CS, and sodium silicate on SSC's compressive strength and hydration mechanism have been investigated experimentally in this study. Results show that using 2% OPC, 2% CS, and 1% sodium silicate as alkaline activators effectively activates slag hydration in SSC-2, achieving a compressive strength of 9.6 MPa at 1 day of hydration. As hydration progresses, SSC's compressive strength continues to increase. In the early hydration stage, OPC and CS create an alkaline environment for SSC, facilitating rapid slag reaction with anhydrite and sodium silicate, resulting in ettringite and C–S–H formation. Simultaneously, slag hydration produces C–S–H and OH-hydrotalcite, filling voids in the ettringite-formed skeleton structure, leading to a denser microstructure and significantly enhancing SSC's early compressive strength. From 28 to 90 days of hydration, the ettringite formation rate decreases in the SSC system, but some anhydrite remains, while C–S–H production continues to rise, further enhancing late-stage compressive strength.

KEYWORDS

super-sulfated cement, ordinary Portland cement, carbide slag, sodium silicate, ettringite, C-S-H

1 Introduction

As global industrialization accelerates, ordinary Portland cement (OPC), one of the most commonly used binders in the construction industry, surpassed production of 4.10 billion tons in 2022 (U.S. Geological Survey, 2023), with anticipated growth in future demand. However, the production process of OPC is characterized by high energy consumption and significant carbon emissions, emitting 800–900 kg of carbon dioxide per ton of

OPC clinker produced (Hasanbeigi et al., 2010; Ali et al., 2011). This scenario has compelled the cement industry to urgently seek solutions to reduce carbon emissions and enhance the efficiency of solid waste resource utilization, particularly in developing new low-carbon cementitious materials.

Industrial production annually generates a significant amount of solid waste, including common by-products like slag from the steel industry and carbide slag (CS) from the chlor-alkali industry. It has been reported that each ton of iron ore can produce 0.5–1.0 tons of slag (Das et al., 2007), with China alone generating over 100 million tons annually, totaling more than 1 billion tons (Guo et al., 2018). CS comprises over 80% dry residue $Ca(OH)_2$, with annual emissions in China exceeding 50 million tons, equivalent to over 100 million tons of alkaline solid waste (Yang et al., 2020). Due to the lack of viable industrial applications, CS is typically disposed of in landfills, resulting in severe environmental pollution, soil and water contamination, and threats to human health and ecosystems (Yang et al., 2014). Therefore, developing low-carbon cementitious materials using industrial by-products as precursors has emerged as the most effective approach to alleviate the environmental pressure of cement production and reduce the demand for traditional cement.

Super-sulfated cement (SSC) has gained attention as a low-carbon cementitious material. Its primary components include 70%–80% granulated blast furnace slag, 5%–20% gypsum or anhydrite as a sulfate activator, and less than 5% as an alkaline activator (Midgley and Pettifer, 1971; Mehrotta et al., 1982; Gruskovnjak et al., 2011). The range of alkaline activators is broad, including options such as OPC (Li et al., 2022), Portland cement (PC) clinker (Cai et al., 2023), KOH (Rubert et al., 2018), NaOH (Gijbels et al., 2020), or lime (Liao et al., 2023). Industrial by-product gypsum, such as flue gas desulfurization gypsum (Jiang et al., 2018) or phosphogypsum (Wang et al., 2022; Liao et al., 2023) can substitute for the sulfate activator, offering a sustainable alternative. In the hydration of SSC, ettringite and C–S–H are the main hydration products (Chen et al., 2023), while OH-hydrotalcite and aluminum hydroxide ($Al(OH)_3$ (am)) are secondary hydration products. Compared to OPC, SSC exhibits several superior properties, such as low heat of hydration (Hewlett, 1998; Cerulli et al., 2003), high late-stage strength, excellent low permeability (Pinto et al., 2020a), and resistance to sulfate attack (Grounds et al., 2003; Pinto et al., 2020b). Furthermore, the production process of SSC is not only straightforward and efficient but also cost-effective and energy-efficient, contributing to reduced environmental burdens and resource and energy consumption (Liao et al., 2023). Therefore, SSC holds significant potential as an environmentally friendly and economically viable alternative to replace OPC in the construction industry.

The practical application of SSC is hindered by its insufficient early-stage strength, primarily due to inadequate matrix hardening, which further affects its durability (Wu et al., 2021). Existing literature has mainly focused on utilizing no more than 5% OPC or PC clinker as an alkaline activator to study its effects on the hydration mechanism, microstructure, and strength of SSC (Masoudi and Hooton, 2019; Sun et al., 2020). It has been found that the deficiency in early strength of SSC is mainly due to the low dissolution rate of slag, which directly limits the formation rate and quantity of hydration products (Gruskovnjak et al., 2008; Masoudi and Hooton, 2019). While increasing the OPC content in SSC can enhance its early strength, it might adversely affect later performance (Matschei et al., 2005; Juenger et al., 2011). In SSC with higher OPC content, the slag surface is more prone to forming ettringite (Matschei et al., 2005) or OH-hydrotalcite (Richardson et al., 1994), leading to increased capillary pore structure, hindering further strength development. Additionally, KOH, as an alkaline activator, has shown effectiveness in improving early strength of SSC. However, a high concentration of KOH in SSC, despite promoting compressive strength growth within the initial 24 h, may result in lower compressive strength after 7 days due to the rapid ettringite formation (Matschei et al., 2005; Rubert et al., 2018). SSC activated with a low concentration of KOH exhibits slower hydration kinetics and gradual early strength increase. Moreover, when NaOH is used as an alkaline activator, its molar concentration significantly influences hydration product formation and the SSC's final performance (Gijbels et al., 2020). A high molar concentration of NaOH facilitates C-A-S-H gel formation, but its highly alkaline conditions raise safety, energy consumption, and carbon emission concerns, contradicting SSC's low-carbon objectives. Therefore, adjusting the pore solution pH emerges as a key strategy to optimize SSC performance, where using sodium lactate and low-concentration sodium citrate as alkaline activators can promote ettringite and C–S–H gel formation, maintaining SSC strength stability (Xing et al., 2023). The chelation effect of sodium lactate on the slag surface accelerates its dissolution rate, improving SSC's mechanical properties (Masoudi and Hooton, 2020; Zhou et al., 2021; Peng et al., 2022). Furthermore, introducing high belite-calcium sulfoaluminate clinker enhances SSC's early strength by accelerating early ettringite formation, offering a practical approach to improve early performance (Sun et al., 2022). However, the strategy of increasing hardening temperature to promote SSC's early strength is economically limited (Angulski da Luz and Hooton, 2015). Thus, developing more sustainable and cost-effective methods to enhance SSC's early performance becomes crucial.

This study devised and implemented a novel activation method to expedite the hydration rate of slag in SSC and enhance its early strength properties. Given the imperative to reduce production costs and carbon footprint, and promote energy conservation and emission reduction, this research explored the efficient utilization of industrial by-product CS. The method meticulously examined the impact of OPC, CS, and sodium silicate as alkaline activators on the hydration mechanism and microstructural changes in the SSC system. In preparing the SSC, 15% natural anhydrite served as a sulfate activator. The mechanical performance of SSC was assessed by measuring compressive strength. Isothermal calorimetry was employed to analyze the hydration kinetics behavior of the SSC paste. The pore structure of the SSC paste was characterized using mercury intrusion porosimetry (MIP). Furthermore, X-ray diffraction (XRD) and Thermogravimetric Analysis (TGA) techniques tracked the phase transitions of the raw reactants and the formation of hydration products. A selective dissolution test was used to test the reaction amount of slag in hardened pastes. Finally, thermodynamic modeling was applied to simulate the hydration mechanism of SSC to achieve a comprehensive understanding of the evolution of various phases within SSC.

2 Experimental

2.1 Materials

The SSC comprised five main constituents: slag, natural anhydrite, OPC, CS, and sodium silicate, with OPC, CS, and sodium silicate serving as alkaline activators, while natural anhydrite acted as a sulfate activator. Commercial industrial-grade sodium silicate with a standard modulus of 2.8 was utilized. The chemical composition of slag, natural anhydrite, OPC, and CS was determined through X-ray fluorescence (XRF) analysis, and the mix proportions of the SSC system are listed in Table 1. The XRD pattern of the slag (see Figure 1) indicated its primarily amorphous nature. The specific surface area of the slag used in this study was measured at 425 m^2/kg. The mineralogical composition of OPC, CS, and natural anhydrite was determined through quantitative XRD analysis refined by the Rietveld method and listed in Table 2. To maintain the workability of the paste and mortar, superplasticizer powder was added to the binder, constituting 0.05 wt% of its total mass.

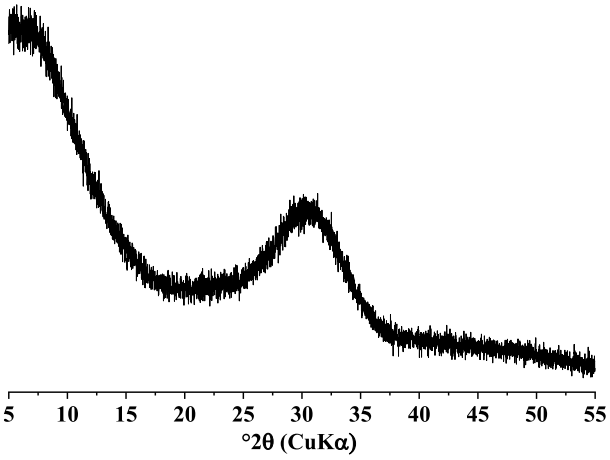

FIGURE 1
X-ray diffraction pattern of slag.

2.2 Sample preparation

In preparing cement paste with a water-to-cement ratio of 0.4, the mixture was initially poured into molds measuring 40 mm × 40 mm × 160 mm. Subsequently, the paste was allowed to cure in a controlled environment within a curing chamber under standard conditions (temperature of 20°C ± 2°C and 95% relative humidity) for 24 h before demolding. Following demolding, the pure cement paste was further cured in water at a temperature of 20°C ± 1°C until it reached the desired age. To term the hydration process of the cement paste, it was crushed into pieces weighing approximately 1 g each, and these pieces were then immersed in isopropanol with a volume ratio of 1:5. The termination of hydration was conducted in two phases: initially, the crushed samples were submerged in isopropanol for 24 h, followed by a transfer to a fresh isopropanol for an additional 48 h immersion. Subsequently, the samples were dried at 40°C for over 3 to remove residual isopropanol. The final step involved the prevention of sample carbonation by grinding the dried samples into a fine powder using an agate mortar and pestle, followed by sieving through a 63-μm square mesh. The sieved powder samples were immediately sealed for subsequent TGA and XRD analysis, while the larger particulate samples were reserved for porosity structure analysis.

2.3 Analytical methods

2.3.1 Compressive strength

This study designed three different proportions of SSC mortar samples, designated as SSC-1, SSC-2, and SSC-3, respectively, along with an OPC mortar sample serving as the control group. Following

TABLE 1 Chemical compositions and mixture proportions of the binder components.

	Chemical composition (wt%)				Mixture proportions (wt%)			
	Slag	Anhydrite	CS	OPC	ID	SSC-1	SSC-2	SSC-3
CaO	40.3	40.69	92.61	63.22	Slag	80	80	80
SiO_2	30.75	2.58	2.82	20.81	Anhydrite	15	15	15
Al_2O_3	14.98	0.4	0.79	4.11	OPC	3	2	1
SO_3	3.15	50.65	1.29	2.08	CS	1	2	3
Fe_2O_3	0.26	0.25	0.17	3.16	SS	1	1	1
MgO	10.22	2.7	1.36	3.19				
TiO_2	0.75	–	–	0.52				
Others	0.59	2.38	0.95	1.12				
SSA (m^2/kg)	425	398	364	358				

TABLE 2 Mineralogical composition of OPC, CS, and anhydrite.

Mineralogical composition (wt%)			
ID	OPC	CS	Anhydrite
C_3S	59.50	–	–
C_2S	17.59	–	–
C_3A	6.38	–	–
C_4AF	12.16	–	–
f-CaO	0.80	–	–
$CaSO_4$	–	–	89.64
$CaSO_4{\cdot}2H_2O$	–	–	5.74
$Ca(OH)_2$	–	83.34	–
$CaCO_3$	–	14.61	3.52
SiO_2	–	2.05	
Other	3.57	–	1.44

the GB/T 17617-1999 standard, "Methods for testing strength of cement mortar," all mortar specimens were prepared with a cement-to-sand ratio of 1:3 and a water-to-cement ratio of 0.5, with each specimen measuring 40 mm × 40 mm × 160 mm. The compressive strength of the specimens was tested using a loading rate of 2400 N/s at curing ages of 1, 3, 7, 14, 28, and 90 days. The compressive strength results were based on the average values from six samples in each group.

2.3.2 Pore structure measurement

The AutoPore IV9500 mercury intrusion porosimeter manufactured by Micromeritics was employed to characterize and analyze the pore structure of hardened cement paste. The volume of the expansion agent used in the experiment was 5cc, and the pore size analysis range was set at approximately 4 nm–30000 nm. Samples with diameters ranging between 5 and 8 mm were selected to determine pore size distribution and porosity, assuming a contact angle of 130° between mercury and the sample surface.

2.3.3 Hydration heat

Utilizing a TAM Air Isothermal Calorimeter, the heat evolution rate and cumulative heat release during cement hydration were measured at a constant temperature of 20°C. The cement mass was controlled at 2.0 ± 0.05 g in the experiments, with a water-to-cement ratio of 0.4. Before the experiments, it was ensured that the surface of the ampoule containing the cement sample and the syringe filled with deionized water were dry. At the start of the experiment, the syringe was affixed atop the ampoule, and then the apparatus was placed within the calorimeter. Once thermal equilibrium was reached, we initiated the process of internal mixing between the cement and deionized water, which continued for 1 minute. The hydration heat testing was conducted for 96 h.

2.3.4 X-ray diffraction

Hydration products of paste samples at different hydration ages were analyzed at room temperature using a Rigaku-Smart-Lab powder diffractometer. The diffractometer utilized CuKα radiation (λ = 1.5405 Å) with a tube current and voltage of 40 mA and 40 kV, respectively. The scanning range was from 5° to 55°, with a step size of 0.0102 and a scanning speed of 1.5°/min, and each scan required approximately 35 min. The amorphous content of the paste samples was calculated using the internal standard method, where the paste samples were mixed with 20% ZnO as an internal standard. Quantitative analysis of the hydration products of paste samples was performed using the TOPAS V7 of the Rietveld method, and crystal structure information for the identified crystalline phases was retrieved from the Inorganic Crystal Structure Database (ICSD).

2.3.5 Thermogravimetric analysis

Thermogravimetric analysis of powder samples was conducted using the Netzsch STA449F3 instrument. Approximately 20 ± 0.3 mg of the sample was placed in an alumina crucible. The heating rate was set at 10 K/min within a temperature range of 30°C–600°C for testing. Nitrogen gas was served as a protective atmosphere throughout the experiment to prevent sample oxidation.

2.3.6 Reaction degree of slag

This study utilized the selective dissolution analysis method on powder paste samples according to the Chinese standard "GB/T 12960-2019" to evaluate the degree of slag hydration. The analysis involved three solutions: 0.15 mol/L EDTA solution, 50 g/L sodium hydroxide solution, and a 33.3% volume ratio of triethanolamine (TEA) solution. Initially, the pH of the selective dissolution solution was adjusted to 11.60 ± 0.05 using a sodium hydroxide solution. Subsequently, 0.30 ± 0.01 g of fine powder (with a particle size less than 63 μm) was added to the selective dissolution solution. The solution with the sample was stirred with a magnetic stirrer for 30 min, followed by two washes of the insoluble residue with isopropanol and filtration. This analysis aimed to selectively dissolve all hydration products and activators, leaving the unreacted slag undissolved. The hydration degree of the slag was calculated using Eq. 1.

$$\alpha_s = \left(1 - \frac{100 \times M_s}{(1 - M_w) M_{s,0} M_{s,e}}\right) \times 100\%, \quad (1)$$

Where α_s: the reaction degree of slag.

Ms: the mass fraction of the dried residue of SSC pastes after EDTA extraction.

Mw: the mass fraction of chemically bound water in SSC pastes at 600°C.

$M_{s,0}$: the mass fraction of slag in SSC.

$M_{s,e}$: the mass fraction of the dried residue in slag.

2.3.7 Thermodynamic modeling

The GEMS-PSI software, widely used in geochemical modeling, was employed for thermodynamic simulations. GEM-Selektor v.3.5 software (Wagner et al., 2012; Kulik et al., 2013), based on the Gibbs free energy minimization principle, facilitated the calculation of equilibrium phase combinations under various environmental conditions (Lothenbach and Gruskovnjak, 2007;

Lothenbach et al., 2008). This study investigated the solid phase composition simulation of the SSC system at 25°C and 1 bar, assuming complete hydration of the cement with a water-to-cement ratio set at 0.4. Thermodynamic data for the solid phases of the SSC system were primarily sourced from the Cemdata18.01 (Lothenbach et al., 2019) and PSI/Nagra thermodynamic databases. The formation process of C–S–H gel was explored using the CSH3T model.

The following assumptions were proposed based on the thermodynamic model of the SSC system hydration:

1. The study assumed that a thermodynamic equilibrium was reached between the precipitated hydration products and the pore solution.
2. The mass change of hydration products was calculated using input data based on a 5% alkali activator and 15% natural anhydrite, along with the slag reaction percentage measured by the EDTA method.
3. The mass changes of the hydration products were computed as a function of the slag dissolution percentage.

3 Results

3.1 Compressive strength

The compressive strength of SSC system mortars and OPC mortar at 1, 3, 7, 14, 28, and 90 days is illustrated in Figure 2. During the early hydration stages, particularly from 1 to 7 days, the compressive strength of SSC system mortars increased rapidly. Notably, after 3 days of hydration, the compressive strength of SSC system mortars surpassed that of OPC mortars. After 3 days of hydration, the SSC-2 mortar, with an alkaline activator formulation of 2% OPC, 2% CS, and 1% SS, exhibited the highest compressive strength, outperforming SSC-1 and surpassing both SSC-3 and OPC. As hydration progressed, SSC system mortars steadily increased in compressive strength. Throughout various testing times, SSC-2 mortar consistently exhibited exceptional compressive strength: it reached 9.6 MPa at 1 day of hydration, slightly below that of OPC mortar; its compressive strength was 27.5 MPa at 3 days of hydration, exceeding OPC mortar by 5.36%; by 7 days of hydration, its compressive strength increased to 42.5 MPa, 7.87% higher than that of OPC mortar; and after 28 days of hydration, the compressive strength of SSC-2 mortar escalated to 63.4 MPa, marking a 20.99% improvement over that of OPC mortar, thus demonstrating the optimal synergistic effect attributed to its unique mixture proportion. In the late hydration stage, from 28 to 90 days, the compressive strength of SSC system mortars continued to show significant growth, with compressive strength of SSC-2 experiencing the most notable increase and the compressive strength of SSC-1 and SSC-3 continuously surpassing that of OPC. During this period, the compressive strength of SSC-1, SSC-2, and SSC-3 increased by 7.91%, 9.62%, and 8.30%, respectively, while that of OPC mortar increased by 9.35%. These results suggest that the growth in compressive strength of the SSC mortars is not directly proportional to the alkaline activator (CS) content, implying that various factors need to be considered when designing SSC formulations to achieve optimal performance.

3.2 Microstructure analysis

The porosity and pore size distribution of the SSC system pastes after 1, 28, and 90 days of hydration are illustrated in Figure 3. In the hardened cement matrix, the pore structure mainly consists

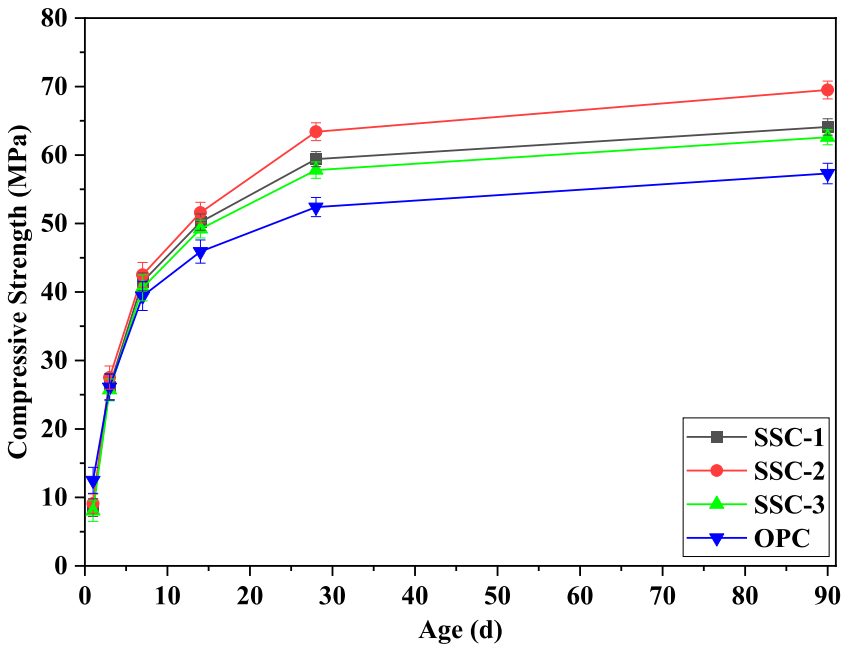

FIGURE 2
Compressive strength development of the SSC system mortars at 1, 3, 7, 14, 28, and 90 days.

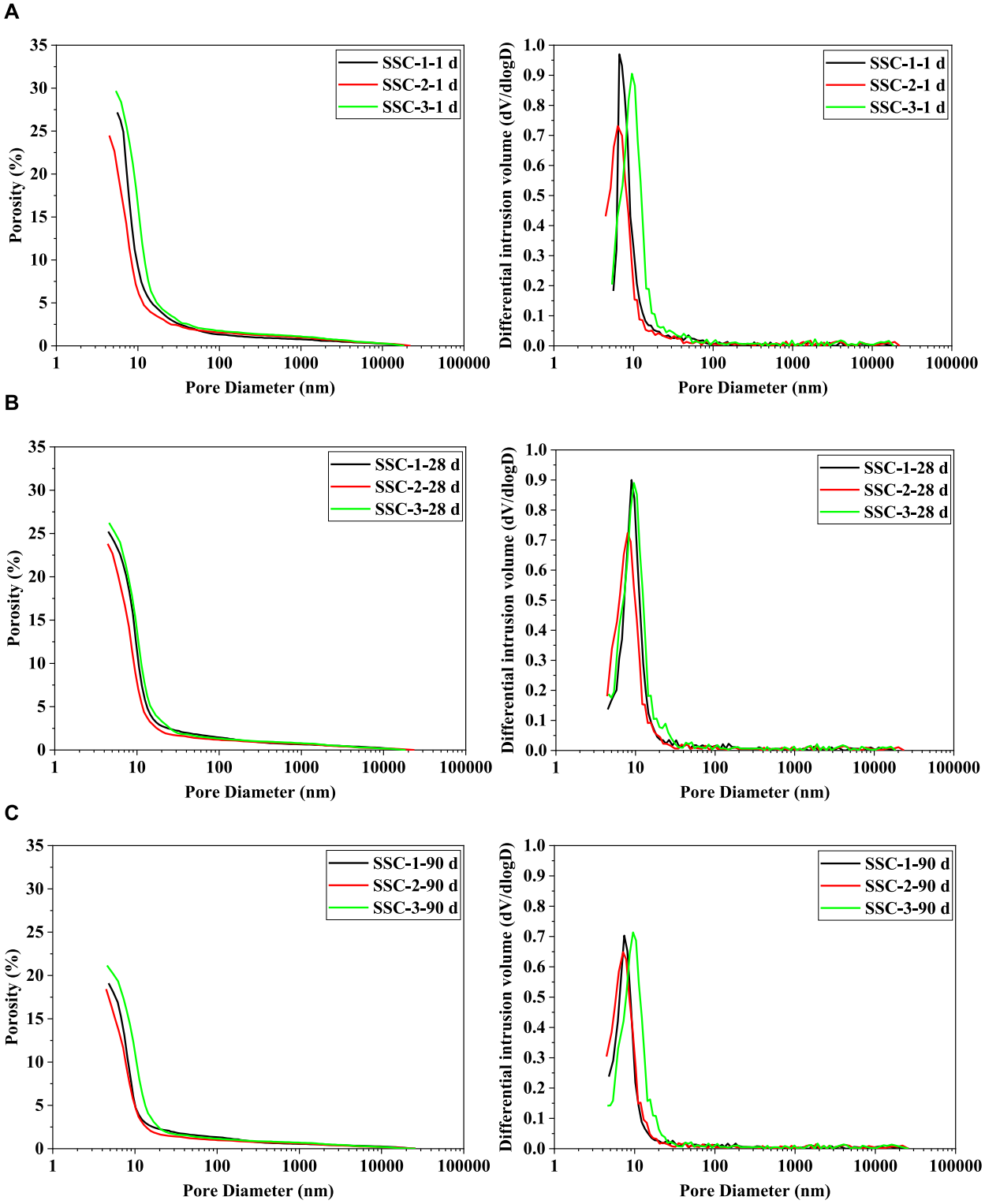

FIGURE 3
Porosity and differential intrusion curve of the SSC system pastes at **(A)** 1 day, **(B)** 28 days, and **(C)** 90 days.

of air voids (larger than 100 nm), capillary pores (50–100 nm), mesopores (4.5–50 nm), and gel pores (less than 4.5 nm) (Wu et al., 2021; Huang et al., 2022). As shown in Figure 3, during the early stages of hydration, particularly at 1 day of hydration, mesopores were the predominant pore size in the SSC system paste, attributed to the rapid hydration of slag with anhydrite and sodium silicate, resulting in the formation of ettringite and C–S–H, while the hydration action of the slag itself also produced C–S–H and

OH-hydrotalcite. These newly formed hydration products filled the pores in the skeleton structure formed by ettringite, thereby creating a denser microstructure and significantly enhancing the early compressive strength. At 1 day of hydration, the SSC-2 paste exhibited low porosity (approximately 24.49%) and the highest compressive strength. As the hydration process progressed, the pore size distribution in the SSC system pastes showed a trend toward smaller pore sizes, thereby reducing the proportion of harmful capillary pores while increasing the proportion of less harmful and harmless pores. After 28 days of hydration, the pore structure of the SSC system pastes primarily transitioned from pores greater than 50 nm to those smaller than 50 nm. By 90 days of hydration, pores smaller than 50 nm accounted for 89.36% of the total pore volume, indicating that with increasing age, the proportion of smaller pores in SSC-1, SSC-2, and SSC-3 pastes gradually increased, which in turn improved their compressive strength. Notably, the significant reduction in the porosity of SSC-2 indicated a notable enhancement in the densification of its hardened matrix.

3.3 Heat hydration

By assessing the hydration evolution rate and cumulative heat of SSC system pastes, the impact of OPC, CS, and sodium silicate as alkaline activators on the hydration kinetics of the SSC system pastes was explored, as depicted in Figure 4. Throughout the 96-h hydration process, the SSC system pastes displayed two notable peaks of hydration heat release. The initial exothermic peak, occurring immediately after paste mixing (0–1.1 h), likely stemmed from the dissolution of reactant phases in the pastes and their wetting action. The second exothermic peak arose between 2.5 and 30.0 h, representing the accelerating stage of paste hydration. Notably, despite adjustments in the proportion of alkaline activators, the duration of the induction stage for all SSC system pastes remained constant, lasting 1.5 h (1.0–2.5 h). The second exothermic peak of the SSC-2 paste demonstrated a faster hydration evolution rate than those of SSC-1 and SSC-3 pastes, with the accelerating stage persisting for 7.8 h (2.5–10.3 h), consistent with its early compressive strength development. Based on these findings, SSC-2 was deemed the optimized mix proportion. With increased CS addition and decreased OPC addition, the cumulative heat of the SSC system pastes initially increased, followed by a decrease, with the SSC-2 paste exhibiting the highest cumulative heat. In the first 24 h of hydration, the cumulative heat of the SSC system pastes rapidly increased, followed by a gradual slowdown in growth rate. This trend indicates that the rapid formation of ettringite is a crucial factor in the early rapid setting and hardening of the SSC pastes, while the late performance gains gradually slowed due to a reduction in the rate of slag dissolution. The 72-h cumulative heat analysis revealed cumulative heats for SSC-1, SSC-2, and SSC-3 of 136.19 J/g, 142.30 J/g, and 133.29 J/g, respectively.

3.4 XRD

Based on the XRD patterns shown in Figure 5 for SSC system pastes at hydration ages of 1, 3, 7, 28, and 90 days, along with the quantitative XRD analysis results depicted in Figure 6, a characteristic amorphous hump was observed within the 2θ angle range of 25°–35°. These amorphous phases primarily consisted of unhydrated slag, along with hydration products such as C–S–H and OH-hydrotalcite. In the SSC systems, ettringite was identified as the main crystalline hydration product, and its formation relied predominantly on the dissolution of slag and the hydration reaction between slag and anhydrite. The quantitative XRD results confirmed that at 1 day of hydration, the SSC-2 paste exhibited a higher formation quantity of ettringite, reaching 19.56%, compared to SSC-1 and SSC-3. From 1 to 7 days of hydration,

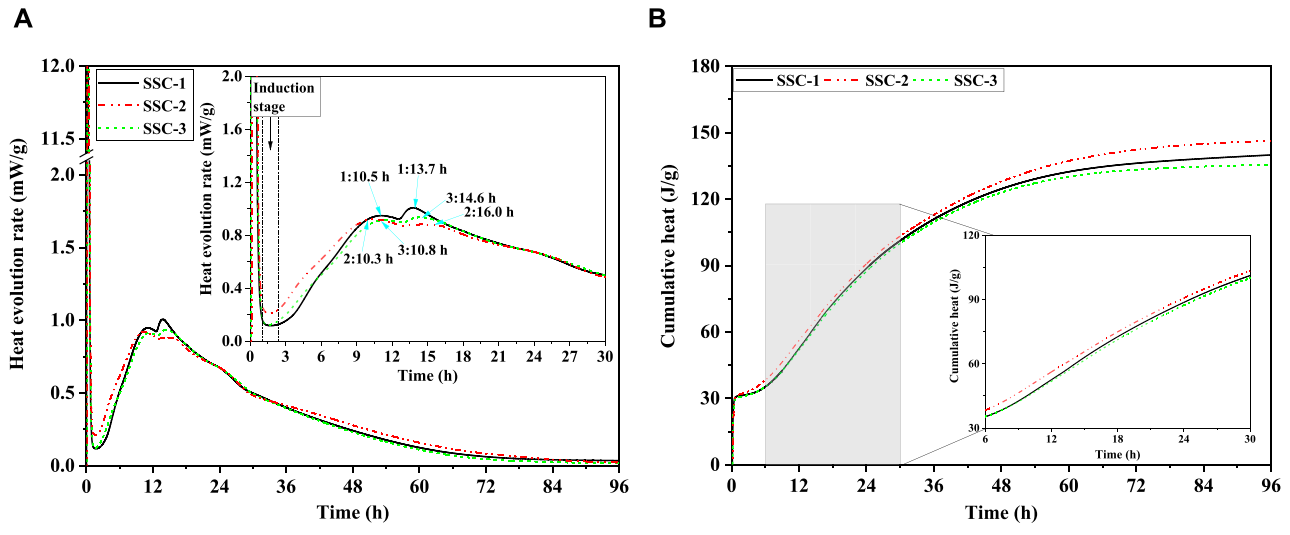

FIGURE 4
Measured hydration heat: **(A)** heat evolution rate; **(B)** cumulative heat.

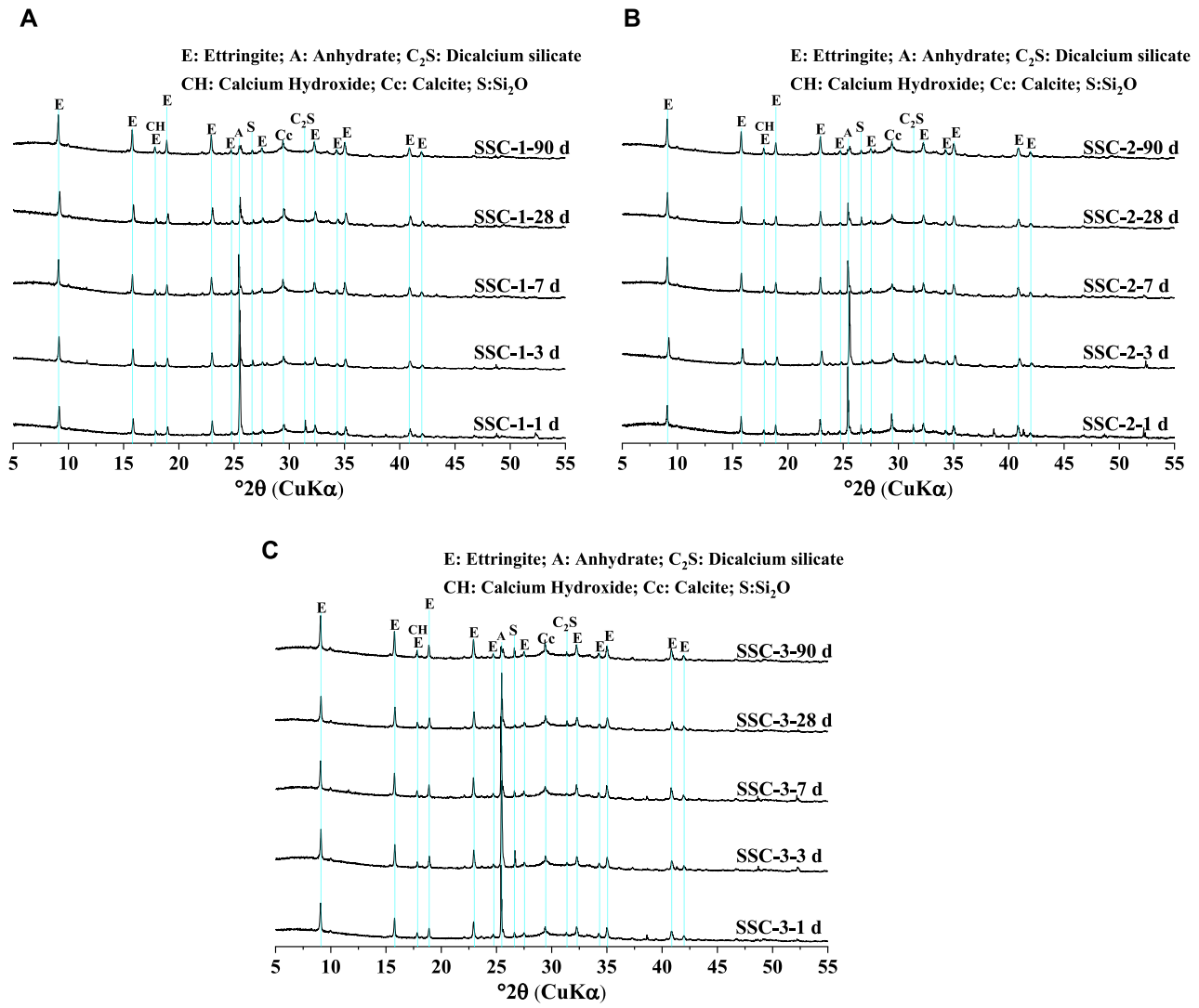

FIGURE 5
XRD patterns of **(A)** SSC-1, **(B)** SSC-2, and **(C)** SSC-3 pastes at 1 day, 3 days, 7 days, 28 days, and 90 days.

the amounts of ettringite formed in SSC-1, SSC-2, and SSC-3 pastes increased by 46.61%, 34.87%, and 50.18%, respectively, indicating a rapid growth trend. This growth trend reflected the promotion of ettringite formation through the hydration reaction between anhydrite and slag. However, as the anhydrite content gradually decreased, the rate of ettringite formation slowed. By 28 days of hydration, the amount of ettringite formed in the SSC-2 paste was the highest compared to SSC-1 and SSC-3, at 27.57%. From 28 to 90 days of hydration, as anhydrite was depleted, the growth rate of ettringite in all pastes declined, with increases in ettringite formation of only 1.35%, 1.20%, and 5.29% for SSC-1, SSC-2, and SSC-3, respectively. Notably, at 90 days of hydration, the characteristic peaks of $Ca(OH)_2$ were not observed in the XRD patterns, indicating that $Ca(OH)_2$ had completely reacted. Considering the difficulty of effectively analyzing amorphous phases such as C–S–H and OH-hydrotalcite via XRD, the TGA technique was employed to further characterize these amorphous materials.

3.5 TGA

The TGA and differential thermogravimetry (DTG) results of the SSC system pastes at different stages of hydration (1, 3, 7, 28, and 90 days) were analyzed, as shown in Figure 7. Within the temperature range of 120°C, a significant endothermic peak was observed, primarily attributed to the loss of non-evaporable water in ettringite and C–S–H. The findings indicated that the main hydration products of the SSC system pastes throughout the hydration process were ettringite (within the 70°C–450°C range) and C–S–H (within the 50°C–600°C range). Notably, in the temperature range of 50°C–400°C, the dehydration curves of ettringite and C–S–H overlapped with those of OH-hydrotalcite, demonstrating the coexistence of these substances. At the initial stage of hydration (1 day), TGA analysis revealed that, compared to SSC-1 and SSC-3 pastes, the SSC-2 paste exhibited a higher mass loss in the temperature range of 30°C–600°C. Quantitative XRD analysis could further confirm this phenomenon, indicating

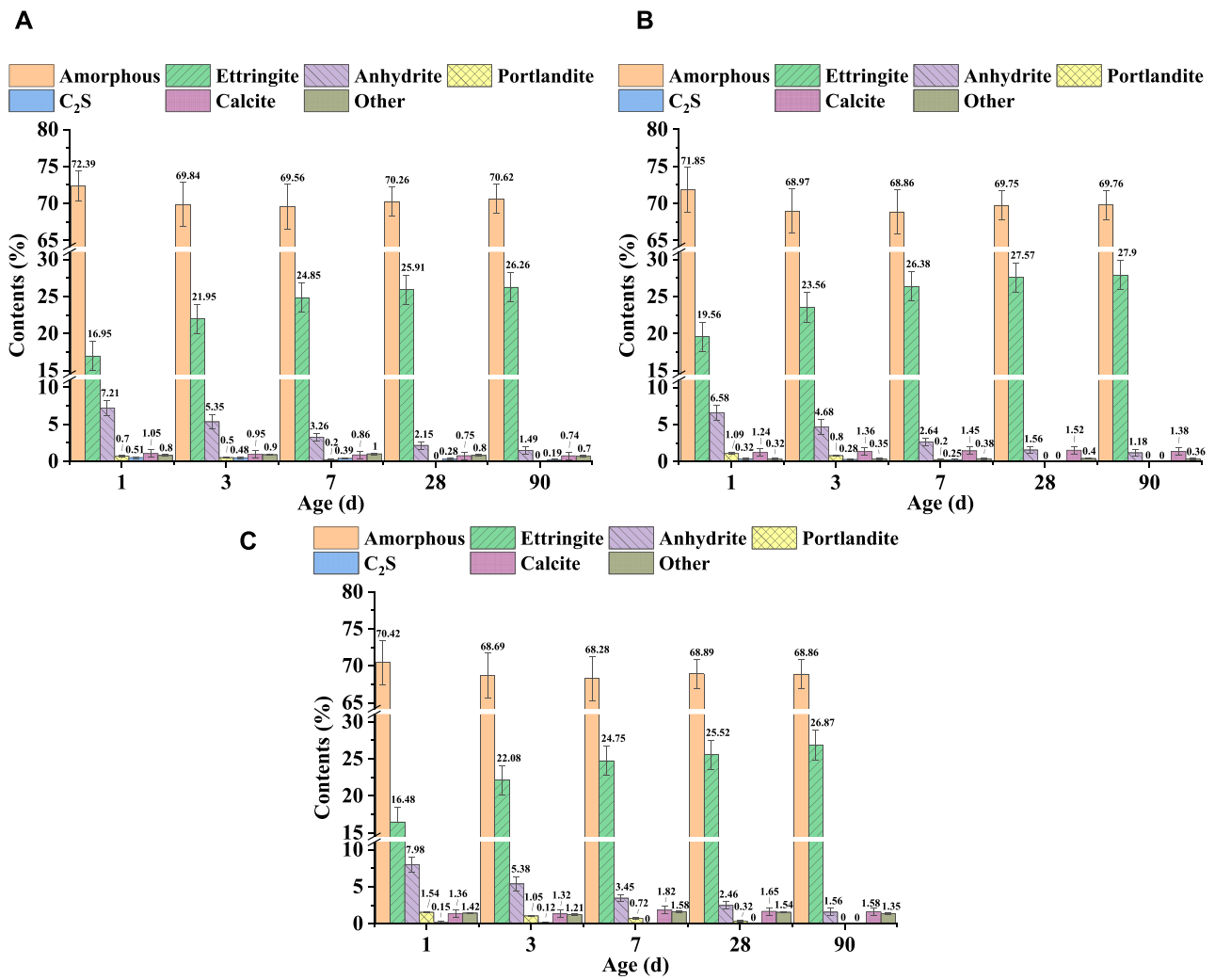

FIGURE 6
Hydration products evolution of **(A)** SSC-1, **(B)** SSC-2, and **(C)** SSC-3 pastes for up to 90 days.

the formation of a greater amount of crystalline hydration products (ettringite) in the SSC-2 paste. As the hydration age increased to 7 days, the amount of ettringite formed in the SSC system pastes rapidly increased, with the SSC-2 paste showing the highest amount of ettringite formation, although the difference compared to SSC-1 and SSC-3 was minimal. From 7 to 28 days of hydration, the rate of ettringite formation in the SSC system pastes slowed down. By 90 days of hydration, as the anhydrite content decreased, the formation rate of ettringite decreased, and the main hydration products in the SSC system pastes transitioned to C–S–H.

Furthermore, the higher mass loss exhibited by the SSC-2 paste in TGA analysis confirmed that alkaline activators containing 2% OPC, 2% CS, and 1% sodium silicate promoted the formation of more hydration products. DTG analysis indicated that, with increasing hydration age, the dehydration weight loss peak of ettringite continued to rise, suggesting a continuous increase in its formation. However, within the first 28 days of hydration, no distinct C–S–H dehydration weight loss peak was observed in the DTG patterns. It was not until 90 days of hydration that the dehydration weight loss peak of C–S–H became prominently visible, marking the formation of a large amount of C–S–H in the late hydration stage. Additionally, as the hydration process progressed, OH-hydrotalcite formation was observed in the SSC system, with its quantity gradually increasing over time. As $Ca(OH)_2$ (400°C–500°C) is minimally present in the CA-CS-SSC system pastes, and its dehydration curve overlaps with those of ettringite, C–S–H, and OH-hydrotalcite, determining its precise content is challenging.

3.6 Reaction degree of slag

Before testing the reaction degree of slag in the SSC system pastes, a selective dissolution method was employed to pretreat the unreacted original slag, determining the content of insoluble

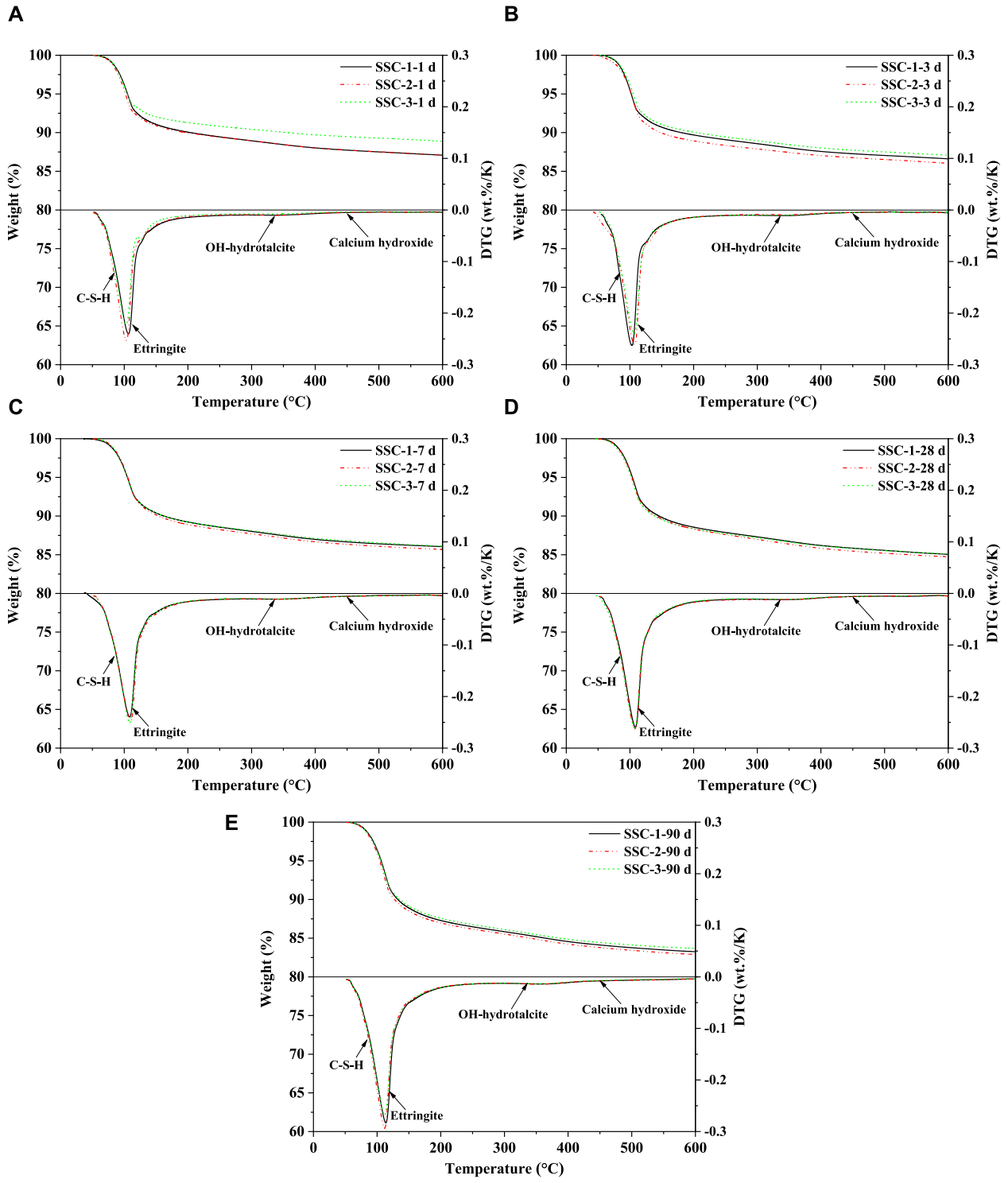

FIGURE 7
TGA and DTG curves of the SSC system paste at **(A)** 1 day, **(B)** 3 days, **(C)** 7 days, **(D)** 28 days, and **(E)** 90 days.

substances and correcting the estimation of unhydrated slag in the SSC system pastes. The reaction degree of slag in the SSC system pastes was tested at hydration stages of 1, 3, 7, 28, and 90 days to quantify the total amount of unhydrated slag. Figure 7 depicts the relationship between the reaction degree of slag and hydration time for the SSC-1, SSC-2, and SSC-3 pastes. TGA was conducted on the solid residues of the EDTA-treated SSC-1, SSC-2, and SSC-3 pastes to ensure all possible hydration products had dissolved, leaving only the unhydrated slag. The experimental results indicated that, compared to SSC-1 and SSC-3, SSC-2 exhibited

10.3389/fmats.2024.1406045

a higher reaction degree of slag at the initial stage of hydration (1 day), reaching 24.29%. Within 7 days of hydration, the reaction degree of slag in the SSC system pastes experienced rapid growth, with the SSC-2 paste showing the highest reaction degree of slag. Specifically, from 1 to 7 days of hydration, the reaction degree of slag in SSC-1, SSC-2, and SSC-3 increased by 86.61%, 75.22%, and 89.93%, respectively. After 7 days of hydration, the growth rate of the reaction degree of slag in the SSC system paste slowed but continued to increase. Despite a decrease in the reaction rate of slag, the reaction degree of slag continued to grow. From 28 to 90 days of hydration, the reaction degree of slag in SSC-1, SSC-2, and SSC-3 pastes increased by 18.53%, 18.09%, and 17.28%, respectively. At 90 days of hydration, the reaction degree of slag in SSC-2 increased to 59.86%, with the reaction degree of slag in SSC-1 and SSC-3 reaching 57.56% and 55.46%, respectively.

3.7 Thermodynamic modeling

Thermodynamic modeling was used to calculate the changes in the quantity of hydration products formed in the SSC system paste as a function of slag dissolution during the hydration process, as illustrated in Figures 8A–C. The input data for the thermodynamic modeling included the reaction degree of slag, anhydrite, OPC, CS, and sodium silicate. These data were based on quantitative results of the XRD-Rietveld analyses (Figures 6A–C) and the reaction degree of the slag (see Figure 9). To accurately calculate the total amount of hydration products formed, it was assumed that the slag dissolved uniformly throughout the hydration process and that thermodynamic equilibrium was reached at each stage. The results predicted by the thermodynamic modeling indicated that the primary hydration products in the SSC system pastes were ettringite, C–S–H, and OH-hydrotalcite. Additionally, the thermodynamic modeling predicted the formation of a minor amount of $C_3(A,F)S_{0.84}H_{4.32}$, a product originating from the hydration of C_4AF in OPC. As C–S–H, OH-hydrotalcite, and $C_3(A,F)S_{0.84}H_{4.32}$ existed in an amorphous state in the SSC system pastes, this structural characteristic made their direct observation using XRD technology relatively challenging. Therefore, the calculation of the amorphous hydration products C–S–H, OH-hydrotalcite, and $C_3(A,F)S_{0.84}H_{4.32}$ in the SSC system pastes by thermodynamic modeling provided a more reliable basis for a deeper understanding of the hydration process in the SSC system. In the thermodynamic modeling calculations for different SSC system pastes (i.e., SSC-1, SSC-2, and SSC-3), it was found that at the early stage of hydration (1 day), the amounts of ettringite and C–S–H generated in SSC-2 exceeded those in SSC-1 and SSC-3, reflecting in the compressive strength performance in the order SSC-2 > SSC-1 > SSC-3. These results from the thermodynamic modeling calculations were consistent with those obtained from XRD and TGA. As the reaction degree of slag increased, the number of hydration products formed increased accordingly. Notably, when the reaction degree of slag exceeded 50%, there was a reduction in the amount of ettringite formed in the SSC-1, SSC-2, and SSC-3 pastes, whereas the amount of C–S–H increased significantly, revealing a relationship between the reaction degree of slag and the number of hydration products formed.

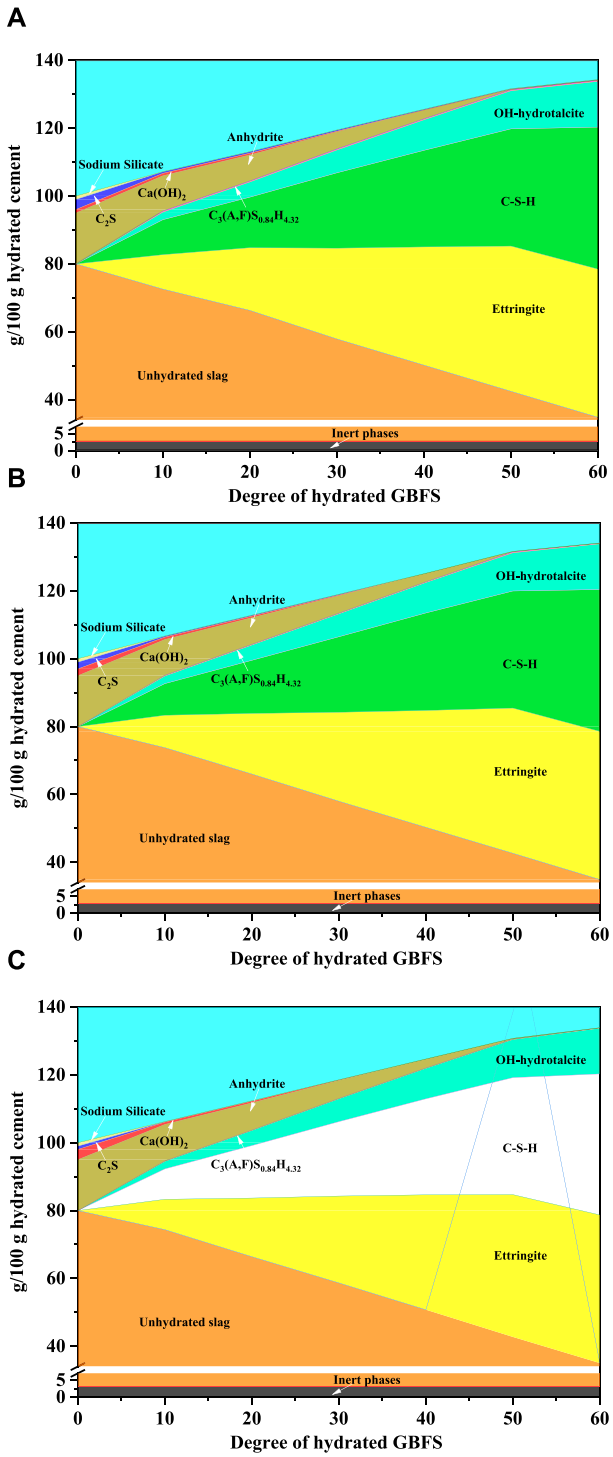

FIGURE 8
Modeled changes of phase messes of **(A)** SSC-1, **(B)** SSC-2, and **(C)** SSC-3 for up to 90 days.

4 Discussion

The slag, primarily composed of CaO, SiO_2, Al_2O_3, and MgO, exhibited significantly enhanced hydration reactivity upon activation in an alkaline pore solution. Upon activation, the slag's

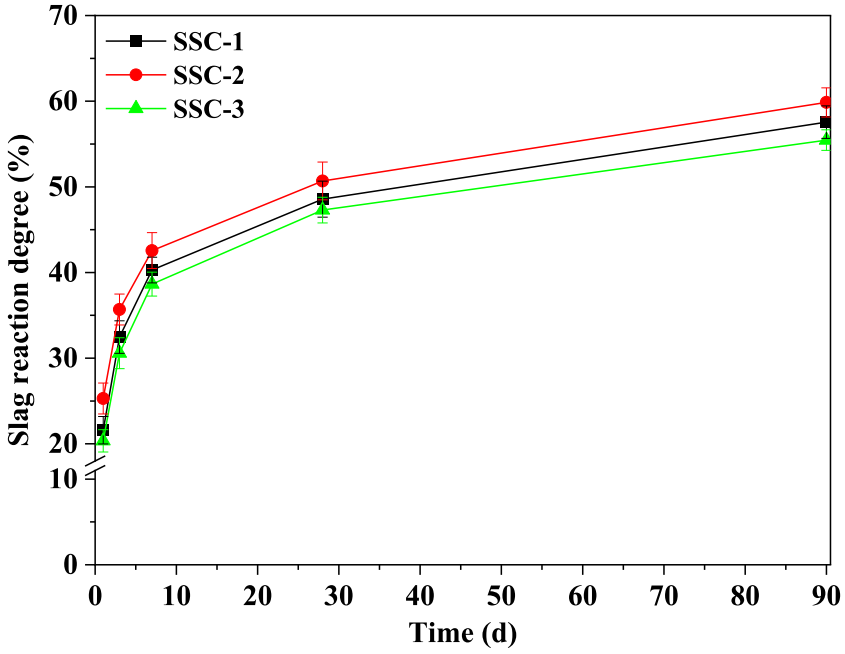

FIGURE 9
Reaction degree of slag in SSC-1, SSC-2, and SSC-3 pastes at 1, 3, 7, 14, 28, and 90 days.

glassy structure dissolved, leading to increased concentrations of calcium, aluminum, and silicon active components in the liquid phase. In the presence of anhydrite, these active components underwent hydration reactions, resulting in the formation of fine crystalline hydration products such as ettringite and C–S–H. These hydration products reduced nucleation barriers, facilitating further slag hydration. Introducing an appropriate amount of sodium silicate into the SSC further enhanced C–S–H formation, thereby improving the microstructure and mechanical properties of the hardened SSC paste.

Research findings indicate that the synergistic interaction among OPC, CS, and sodium silicate significantly promotes slag hydration. The dissolution of CS and OPC releases calcium hydroxide, creating the necessary alkaline environment for slag hydration. This not only accelerates slag hydration but also promotes its reaction with anhydrite to form ettringite while facilitating the formation of C–S–H and OH-hydrotalcite, which is crucial for enhancing early strength in the SSC system. Moreover, this synergy optimizes the microstructure of the SSC system by regulating the types and proportions of hydration products, increasing matrix density, and reducing porosity. Compared to merely increasing the content of alkaline compounds, this approach demonstrates greater efficacy in promoting hydration product generation and enhancing the early strength of hardened mortar.

By adjusting the proportions of OPC and CS as alkaline activators, the formation of hydration products and pore structure in the hardened paste could be more optimally controlled, enhancing the microstructure and early mechanical properties of the SSC matrix. With increased CS content and decreased OPC content, the hydration heat release of the SSC system pastes initially increased before decreasing. Specifically, the SSC-2 paste, containing 2% OPC, 2% CS, and 1% sodium silicate as alkaline activators, showed the highest cumulative heat release during hydration, indicating the formation of more hydration products. These products were characterized by a uniform distribution of C–S–H and ettringite, reduced paste porosity, optimized pore size distribution, and formed a denser microstructure. The compressive strength of SSC-2 mortar increased by 342.71% from 1 to 7 days of hydration and 130.55% from 7 to 28 days.

The rapid increase in compressive strength of SSC-2 mortar during the early stage of hydration can be primarily attributed to the rational proportion of alkaline activators, which effectively promote extensive slag hydration and generate a large volume of hydration products. These hydration products optimize the pore structure and result in a denser microstructure, significantly enhancing the early compressive strength of the mortar. However, during the late stage of hydration, the rate of increase in compressive strength of SSC-2 mortar gradually slows down due to the progression of hydration and the influence of ion diffusion coefficients. XRD and TGA results further confirm this trend, showing a gradual decrease in the rate of ettringite formation in the SSC-2 matrix from 28 to 90 days, while the growth rate of the compressive strength of SSC-2 mortar drops to just 9.62%. The increase in compressive strength during the late stage of hydration is primarily influenced by the amount of C–S–H produced, consistent with previous research findings (Sun et al., 2022). In a lower alkalinity environment, the late-stage strength gain of SSC is inhibited, mainly due to the slow diffusion speed of silicate ions, leading to the formation of a layer rich in silicon and aluminum around the dissolved slag particles. This causes C–S–H to precipitate around the slag, hindering the diffusion rate of free water to the slag surface

(Skibsted and Snellings, 2019), ultimately reducing the dissolution of the slag.

Furthermore, compared to the OPC reference, the heat released in the SSC is significantly lower, demonstrating low-heat cement properties while maintaining high early and late strength. For example, the SSC-2, comprising 2% OPC, 2% CS, and 1% sodium silicate as alkaline activators, can achieve a strength grade of 52.5R, with a total heat release of 142 J/g of the binder at 3 days of hydration. Given the low hydration heat characteristic of SSC, it offers cementitious material support for addressing the issue of thermal cracking in large-volume concrete.

5 Conclusion

The investigative findings enrich the understanding of revitalizing SSC adhesives using alkali-containing solid waste materials and reveal the potential for utilizing multiple solid waste materials for SSC preparation in future endeavors. Through meticulous experimental examination, this study scrutinized the impact of OPC, CS, and sodium silicate on the hydration and hardening attributes of SSC, leading to the following conclusions:

The proportions of OPC, CS, and sodium silicate as alkaline activators significantly impact the compressive strength and hydration mechanism in the SSC system. As the CS content increased and the corresponding OPC content decreased, the cumulative heat evolution of the SSC system pastes initially increased before decreasing. Particularly, the SSC-2 paste, comprising 2% OPC, 2% CS, and 1% sodium silicate as alkaline activators, showed the highest cumulative heat evolution during hydration. An analysis of the hydration mechanism of SSC-2 revealed a significant enhancement in both early and late compressive strengths compared to SSC-1 and SSC-3. This improvement is primarily attributed to the early hydration stage, where the dissolution of CS and OPC produced calcium hydroxide, creating an alkaline environment for the dissolution of fine slag particles and facilitating a rapid reaction with anhydrite to produce a large amount of ettringite and C–S–H. The hydration of fine slag particles also generated hydration products such as C–S–H and OH-hydrotalcite, which effectively filled the pores created by ettringite formation, enhancing the early microstructure of SSC-2 and improving its early compressive strength. As the hydration process progressed, the continuous consumption of anhydrite led to a gradual decrease in the formation rate of ettringite, making C–S–H the dominant hydration product in the SSC system during the late hydration stage, thereby promoting the development of late-stage compressive strength in the SSC system.

The additional proportions of OPC and CS significantly affect the early formation of ettringite in the SSC system. Higher CS content in the SSC causes a delayed hydration effect of the slag, unlike lower CS content in the SSC, which results in a greater amount of ettringite and amorphous hydration products, such as C–S–H and OH-hydrotalcite. As CS content increased, the production of ettringite, C–S–H, and OH-hydrotalcite in the SSC system initially increased before decreasing, with porosity following a similar trend.

Data availability statement

The original contributions presented in the study are included in the article/Supplementary material, further inquiries can be directed to the corresponding author.

Author contributions

GQ: Data curation, Funding acquisition, Project administration, Writing–original draft, Writing–review and editing. QZ: Project administration, Supervision, Writing–review and editing. ZS: Conceptualization, Methodology, Writing–review and editing.

Funding

The author(s) declare that financial support was received for the research, authorship, and/or publication of this article. This work was financially supported by the National Key Research and Development Plan of China (Grant No. 2022YFB2603000).

Conflict of interest

The authors declare that the research was conducted in the absence of any commercial or financial relationships that could be construed as a potential conflict of interest.

Publisher's note

References

Ali, M. B., Saidur, R., and Hossain, M. S. (2011). A review on emission analysis in cement industries. *Renew. Sustain. Energy Rev.* 15 (5), 2252–2261. doi:10.1016/j.rser.2011.02.014

Angulski da Luz, C., and Hooton, R. D. (2015). Influence of curing temperature on the process of hydration of supersulfated cements at early age. *Cem. Concr. Res.* 77, 69–75. doi:10.1016/j.cemconres.2015.07.002

Cai, T. Z., Hou, P. K., Chen, H., Zhao, P. Q., Du, P., Wang, S. D., et al. (2023). Effects of nanosilica on supersulfated cements of different clinker-activation degree. *Constr. Build. Mater.* 365, 130118. doi:10.1016/j.conbuildmat.2022.130118

Cerulli, T., Pistolesi, C., Maltese, C., and Salvioni, D. (2003). Durability of traditional plasters with respect to blast furnace slag-based plaster. *Cem. Concr. Res.* 33 (9), 1375–1383. doi:10.1016/S0008-8846(03)00072-3

Chen, H., Hou, P. K., Zhou, X. M., Black, L., Adu-Amankwah, S., Feng, P., et al. (2023). Toward performance improvement of supersulfated cement by nano silica: asynchronous regulation on the hydration kinetics of silicate and aluminate. *Cem. Concr. Res.* 167, 107117. doi:10.1016/j.cemconres.2023.107117

Gijbels, K., Pontikes, Y., Samyn, P., Schreurs, S., and Schroeyers, W. (2020). Effect of NaOH content on hydration, mineralogy, porosity and strength in alkali/sulfate-activated binders from ground granulated blast furnace slag and phosphogypsum. *Cem. Concr. Res.* 132, 106054. doi:10.1016/j.cemconres.2020.106054

Grounds, T., Nowell, D. V., and Wilburn, F. W. (2003). Resistance of supersulfated cement to strong sulfate solutions. *J. Therm. Anal. Calorim.* 72 (1), 181–190. doi:10.1023/A:1023928021602

Gruskovnjak, A., Lothenbach, B., Winnefeld, F., Figi, R., Ko, S.-C., Adler, M., et al. (2008). Hydration mechanisms of super sulphated slag cement. *Cem. Concr. Res.* 38 (7), 983–992. doi:10.1016/j.cemconres.2008.03.004

Gruskovnjak, A., Lothenbach, B., Winnefeld, F., Münch, B., Figi, R., Ko, S.-C., et al. (2011). Quantification of hydration phases in supersulfated cements: review and new approaches. *Adv. Cem. Res.* 23 (6), 265–275. doi:10.1680/adcr.2011.23.6.265

Guo, J. L., Bao, Y. P., and Wang, M. (2018). Steel slag in China: treatment, recycling, and management. *Waste Manage.* 78, 318–330. doi:10.1016/j.wasman.2018.04.045

Hasanbeigi, A., Price, L., Lu, H. Y., and Lan, W. (2010). Analysis of energy-efficiency opportunities for the cement industry in Shandong Province, China: a case study of 16 cement plants. *Energy* 35, 3461–3473. doi:10.1016/j.energy.2010.04.046

Hewlett, P. C. (1998). *Lea's chemistry of cement and concrete*. fourth ed. New York: Wiley, 664–673.

Jiang, L. H., Li, C. Z., Wang, C., Xu, N., and Chu, and H. Q. (2018). Utilization of flue gas desulfurization gypsum as an activation agent for high-volume slag concrete. *J. Clean. Prod.* 205, 589–598. doi:10.1016/j.jclepro.2018.09.145

Juenger, M. C. G., Winnefeld, F., Provis, J. L., and Ideker, J. H. (2011). Advances in alternative cementitious binders. *Cem. Concr. Res.* 41 (12), 1232–1243. doi:10.1016/j.cemconres.2010.11.012

Kulik, D. A., Wagner, T., Dmytrieva, S. V., Kosakowski, G., Hingerl, F. F., Chudnenko, K. V., et al. (2013). GEM-Selektor geo-chemical modeling package: revised algorithm and GEMS3K numerical kernel for coupled simulation codes. *Comput. Geosci.* 17, 1–24. doi:10.1007/s10596-012-9310-6

Li, B. B., Hou, P. K., Chen, H., Zhao, P. Q., Du, P., Wang, S. D., et al. (2022). GGBS hydration acceleration evidence in supersulfated cement by nano SiO_2. *Cem. Concr. Compos.* 132, 104609. doi:10.1016/j.cemconcomp.2022.104609

Liao, Y. S., Yao, J. X., Deng, F., Li, H., Wang, K. J., and Tang, S. W. (2023). Hydration behavior and strength development of supersulfated cement prepared by calcined phosphogypsum and slaked lime. *J. Build. Eng.* 80, 108075. doi:10.1016/j.jobe.2023.108075

Lobato, N. C. C., Villegas, E. A., and Mansu, M. B. (2015). Management of solid wastes from steelmaking and galvanizing processes: a brief review. *Resour. Conserv. Recycl.* 102, 49–57. doi:10.1016/j.resconrec.2015.05.025

Lothenbach, B., and Gruskovnjak, A. (2007). Hydration of alkali-activated slag: thermodynamic modelling. *Adv. Cem. Res.* 19, 81–92. doi:10.1680/adcr.2007.19.2.81

Lothenbach, B., Kulik, D., Matschei, T., Balonis, M., Baquerizo, L., Dilnesa, B. Z., et al. (2019). Cemdata18: a chemical thermodynamic database for hydrated Portland cements and alkali-activated materials. *Cem. Concr. Res.* 115, 472–506. doi:10.1016/j.cemconres.2018.04.018

Lothenbach, B., Matschei, T., Möschner, G., and Glasser, F. P. (2008). Thermodynamic modelling of the effect of temperature on the hydration and porosity of Portland cement. *Cem. Concr. Res.* 38 (1), 1–18. doi:10.1016/j.cemconres.2007.08.017

Lothenbach, B., and Wieland, E. (2006). A thermodynamic approach to the hydration of sulphate-resisting Portland cement. *Waste Manage* 26, 706–719. doi:10.1016/j.wasman.2006.01.023

Masoudi, R., and Hooton, R. D. (2019). Examining the hydration mechanism of supersulfated cements made with high and low-alumina slags. *Cem. Concr. Compos.* 103, 193–203. doi:10.1016/j.cemconcomp.2019.05.001

Masoudi, R., and Hooton, R. D. (2020). Influence of alkali lactates on hydration of supersulfated cement. *Constr. Build. Mater.* 239, 117844. doi:10.1016/j.conbuildmat.2019.117844

Matschei, T., Bellmann, F., and Stark, J. (2005). Hydration behaviour of sulphate-activated slag cements. *Adv. Cem. Res.* 17 (4), 167–178. doi:10.1680/adcr.2005.17.4.167

Mehrotta, V. P., Sai, A. S. A., and Kapur, P. C. (1982). Plaster of Paris activated supersulfated slag cement. *Cem. Concr. Res.* 12 (4), 463–473. doi:10.1016/0008-8846(82)90061-8

Midgley, H. G., and Pettifer, K. (1971). The microstructure of hydrated super sulphated cement. *Cem. Concr. Res.* 1 (1), 101–104. doi:10.1016/0008-8846(71)90086-X

Peng, Z. C., Zhou, Y., Wang, J. W., Chen, L. C., and Miao, C. W. (2022). The impediment and promotion effects and mechanisms of lactates on the hydration of supersulfated cements - aiming at a performance enhancement. *J. Clean. Prod.* 341, 130751. doi:10.1016/j.jclepro.2022.130751

Pinto, S. R., Angulski da Luz, C., Munhoz, G. S., and Medeiros-Junior, R. A. (2020a). Resistance of phosphogypsum-based supersulfated cement to carbonation and chloride ingress. *Constr. Build. Mater.* 263, 120640. doi:10.1016/j.conbuildmat.2020.120640

Pinto, S. R., Angulski da Luz, C., Munhoz, G. S., and Medeiros-Junior, R. A. (2020b). Durability of phosphogypsum-based supersulfated cement mortar against external attack by sodium and magnesium sulfate. *Cem. Concr. Res.* 136, 106172. doi:10.1016/j.cemconres.2020.106172

Richardson, I. G., Brough, A. R., Groves, G. W., and Dobson, C. M. (1994). The characterization of hardened alkali-activated blast-furnace slag pastes and the nature of the calcium silicate hydrate (C–S–H) phase. *Cem. Concr. Res.* 24 (5), 813–829. doi:10.1016/0008-8846(94)90002-7

Rubert, S., Luz, C. A. D., Varela, M. V. F., Pereira Filho, J. I., and Hooton, R. D. (2018). Hydration mechanisms of supersulfated cement: the role of alkali activator and calcium sulfate content. *J. Therm. Anal. Calorim.* 134 (2), 971–980. doi:10.1007/s10973-018-7243-6

Skibsted, J., and Snellings, R. (2019). Reactivity of supplementary cementitious materials (SCMs) in cement blends. *Cem. Concr. Res.* 124, 105799. doi:10.1016/j.cemconres.2019.105799

Sun, H., Qian, J. S., Yang, Y., Fan, C. H., and Yue, Y. F. (2020). Optimizationof gypsum and slag contents in blended cement containing slag. *Cem. Concr. Compos.* 112, 103674. doi:10.1016/j.cemconcomp.2020.103674

Sun, Z. N., Nie, S., Zhou, J., Li, H., Chen, Z. F., Xu, M. F., et al. (2022). Hydration mechanism of calcium sulfoaluminate-activated supersulfated cement. *J. Clean. Prod.* 333, 130094. doi:10.1016/j.jclepro.2021.130094

U.S. Geological Survey (2023). *Mineral commodity summaries 2023*. Reston, VA: U.S. Geological Survey, 214. Available at: https://www.usgs.gov/publications/mineral-commodity-summaries-2023 (Accessed January 31, 2023). doi:10.5066/P9WCYUI6

Wagner, T., Kulik, D. A., Hingerl, F. F., and Dmytrieva, S. V. (2012). GEM-Selektor geochemical modeling package: TSolMod library and data interface for multicomponent phase models. *Can. Mineral.* 50, 1173–1195. doi:10.3749/canmin.50.5.1173

Wang, Y. B., Xu, L., He, X. Y., Su, Y., Miao, W. J., Strnadel, B., et al. (2022). Hydration and rheology of activated ultra-fine ground granulated blast furnace slag with carbide slag and anhydrous phosphogypsum. *Cem. Concr. Compos.* 133, 104727. doi:10.1016/j.cemconcomp.2022.104727

Wu, Q. Y., Xue, Q. Z., and Yu, Z. Q. (2021). Research status of super sulfate cement. *J. Clean. Prod.* 294, 126228. doi:10.1016/j.jclepro.2021.126228

Xing, J. R., Zhou, Y., Peng, Z. C., Wang, J. W., Jin, Y. J., and Jin, M. (2023). The influence of different kinds of weak acid salts on the macro-performance, micro-structure, and hydration mechanism of the supersulfated cement. *J. Build. Eng.* 66, 105937. doi:10.1016/j.jobe.2023.105937

Yang, H., Cao, J. W., Wang, Z., Chen, H. H., and Gong, X. Z. (2014). Discovery of impurities existing state in carbide slag by chemical dissociation. *Int. J. Min. Process.* 130, 66–73. doi:10.1016/j.minpro.2014.05.003

Yang, J., Liu, S. Y., Ma, L. P., Zhao, S. Q., Liu, H. P., Dai, Q. X., et al. (2020). Mechanism analysis of carbide slag capture of CO_2 via a gas-liquid-solid three-phase fluidization system. *J. Clean. Prod.* 279, 123712. doi:10.1016/j.jclepro.2020.123712

Zhou, Y., Peng, Z. C., Chen, L. C., Huang, J. L., and Ma, T. (2021). The influence of two types of alkali activators on the microstructure and performance of supersulfated cement concrete: mitigating the strength and carbonation resistance. *Cem. Concr. Compos.* 118, 103947. doi:10.1016/j.cemconcomp.2021.103947